HAPSEA: Hydraulically Amplified Soft Electromagnetic Actuator for Haptics

Noah D. Kohls[†‡*], Nicholas Colonnese[†], Yi Chen Mazumdar[‡], Priyanshu Agarwal[†]

Abstract—Novel actuators that can provide squeeze, vibration, and localized forces while remaining soft and comfortable are essential for next-generation augmented reality applications. Despite this need, there are currently few soft actuator topologies that can provide high forces and high bandwidths at low voltages and temperatures. In this work, we present a new type of soft electromagnetic actuator architecture for haptics. These low-cost, easy-to-manufacture, and conformal actuators are composed of a coil, magnet, thin film material, and water. Adding a thin ferromagnetic sheet further enables the creation of a latching actuator variant, which can improve force output while reducing power consumption. Each actuator combines low voltage (up to 2 V), high bandwidth electromagnetics with hydraulics to amplify force output. In addition to force amplification, the hydraulics provide cooling and thermal mass, which enable the actuator to be used safely in wearables for longer durations. In this work, we characterize the output forces, frequency response, efficiency, and thermal profiles of the prototype actuators. Results from tabletop experiments show that with hydraulic amplification, a non-latching actuator is able to exert 1.3 N of force at 4 A and a latching actuator is able to exert up to 5.2 N when preloaded with 3.7 N of compression. Furthermore, the prototype actuator has a bandwidth of 30 Hz when operating in air. After 120 seconds of continuous operation (1.3 W) in ambient air (26°C), the maximum actuator temperature reaches 36°C, making it safe for haptic applications. Using these designs, we develop a prototype wearable wristband device that can render body-grounded squeeze and vibration. By expanding on the operating principles described in this work, novel augmented reality applications can potentially become possible.

Index Terms—wristband, soft actuator, electromagnetic actuator, hydraulic amplification, squeeze, vibration, water cooling

I. Introduction

ADVANCES in augmented and virtual reality (AR/VR) have led to increased demand for haptic devices to supplement visual and audio elements. Haptic feedback can improve the user's ability to manipulate virtual objects [1], enhance realism of virtual environments [2], close the action-confirmation loop in user interfaces [3], and provide feedback to augment or substitute sensation [4]. Haptics therefore, reduces cognitive load, increases reaction speed, and creates a more engaging experience. Many tactile haptic systems currently use vibrational actuators because vibrations are easy to generate, do not require body-grounding, and are readily recognized by users. However, prior work has shown
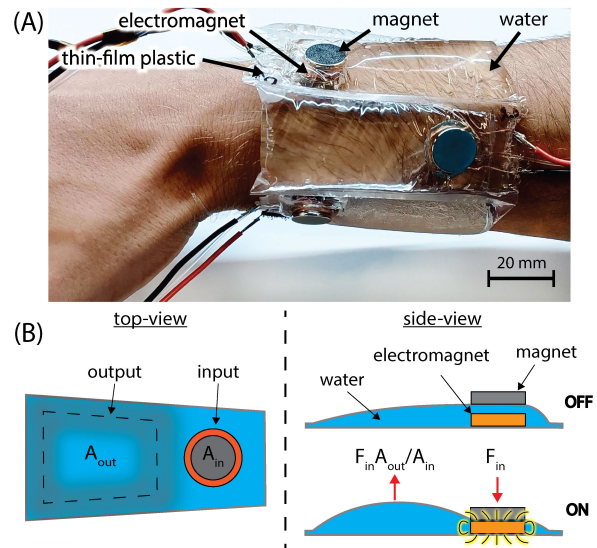

Fig. 1. (A) Haptic wrist device concept with several HAPSEAs is shown. (B) The device is flexible and renders squeeze, vibration, and local force capabilities. When the electromagnet is energized, the attraction force between the magnet and coil is amplified at the output location.

that vibrotactile haptic feedback combined with wrist-based squeeze substantially improves virtual hand-based interactions in AR/VR [5]. Thus, researchers have developed different servo-based mechanisms that render squeeze to grab attention [6] or guide a user's wrist through movement tasks [7], [8]. Developing devices that can render both squeeze and vibration has been an ongoing challenge. One approach [9] has been to develop a wristband device with two actuators, a cable tensioning mechanism for squeeze and hard embedded vibrotactors along the circumference of the wrist for vibration. While both modes of feedback are achievable, using two types of actuators adds complexity. Additionally, the mismatch in mechanical impedance between the rigid haptic device and soft skin leads to comfort and encumbrance issues, which has led to the use of soft elements and actuators [10], [11].

Using soft components, squeeze actuation has been achieved through the use of pneumatic bellows [12] and elastic tubes [13]. Pneumatic actuation, however, requires bulky pressure sources (which hinder portability), employs noisy valves, and has low mechanical bandwidth. Shape memory alloys have also been investigated for soft actuators [14] and haptic squeeze [15], but generate excessive heat for continuous or repeated actuation. Active cooling has also been employed to improve thermal performance [16] and develop wearable devices [17], but these systems remain slow and bulky.

Electromagnetic actuators, on the other hand, are more common in haptic devices due to their high speeds, large forces, and excellent efficiencies [18], [19]. Rigid motors, pumps, and

*Corresponding author: nkohls3@gatech.edu
†Reality Labs Research, Meta Platforms Inc., Redmond, WA 98052, USA. (e-mail: ncolonnese@meta.com, pagarwal18@meta.com)
‡Georgia Institute of Technology, Dept. of Mechanical Engineering, Atlanta, GA, 30332. (e-mail: ellen.mazumdar@gatech.edu)

solenoids, however, have higher mechanical impedances than human skin, requiring soft coupling elements that improve comfort but also dampen the actuator output. One alternative solution has been the development of novel, fully-soft electromagnetic actuators using embroidered coils [20] and liquid metals [21]–[23]. While these actuators are soft and fast, they have high operating temperatures and low output forces.

One approach to improving output force while maintaining high bandwidths and low operating temperatures is force amplification. While there are several interesting amplification techniques like pulley systems [20], many do not translate well to wearable designs. Hydraulic force amplification, on the other hand, has been successfully demonstrated for haptics with soft HASEL (hydraulically amplified self-healing electrostatic) actuators [24]. Using electrostatic attraction, these systems amplify forces by pressurizing a fluid to change the actuator's shape. While this is beneficial in wearables [25], electrostatic and dielectric [26], [27] actuators require high voltages (>1000 V), which can potentially shock users.

In this paper, we present HAPSEA (**H**ydraulically **AmP**lified **S**oft **E**lectromagnetic **A**ctuator), a new type of soft actuator that combines electromagnetic actuation with hydraulic force amplification. This concept, illustrated in Fig. 1, has several contributions including:

- The first demonstration of a compliant multi-modal haptic actuator using a hydro-electromagnetic actuation concept. Aside from flexible membrane pumps [28], hydro-electromagnetic actuators have not been previously proposed in the literature for haptic applications.
- The combined ability to generate high squeeze and local forces as well as high vibration bandwidths for haptics using a single compact hydraulically amplified electromagnetic actuator. The summary in Table I presents the approximate bandwidths and output forces for various actuator designs. This highlights how HAPSEA is able to produce both high forces and frequencies.
- The unique use of hydraulics on an electromagnetic actuator for amplifying force, achieving high bandwidths, regulating temperature, and improving comfort.
- The combination of several HAPSEAs using low-cost and easy-to-fabricate techniques shows how a novel soft haptic wristband device can be created.

Here, we first describe models for the electromagnetic force output and force amplification. Then, the design and manufacturing techniques needed to build the system are discussed. This is followed by characterization of the mechanical dy-

namics, actuator efficiency, and thermal performance. Finally, we conclude by demonstrating the application of the actuator in a haptic wrist device. This application illustrates how the principles discussed in this work can be further optimized for future augmented reality systems and wearable technologies.

II. HYDRO-ELECTROMAGNETIC ACTUATOR MODELING

Figure 1(B) illustrates the basic operation of the soft actuator, which converts electrical energy into hydraulically amplified mechanical force using a planar coil configuration. In this concept, forces are generated by applying current (I) to the electromagnetic coil, thereby generating an induced magnetic field. This, in turn, interacts with the field of the permanent magnet via the Lorentz force, $\vec{F_0} = I\vec{l} \times \vec{B}$. Here, the force output of the coil ($\vec{F_0}$) is proportional to the current and the cross product between the length vector of the wire $\vec{l}$ and the magnetic field of the permanent magnet $\vec{B}$.

In order to more accurately model the interaction between the electromagnetic coil and the cylindrical magnet, the filament method [30] is utilized. In this model, the coil and magnet are simplified and represented as a collection of individual current-carrying loops. The total force between the coil and magnet is calculated as the sum of the forces between each loop. The force per loop in the axial direction is,

$$F_f(r_1, r_2, x) = \mu_0 I_1 I_2 x \sqrt{\frac{m}{4 r_1 r_2}} \left(\mathrm{K}(m) - \frac{m-2}{2(m-1)} \mathrm{E}(m) \right). \quad (1)$$

Here, μ_0 is the magnetic permeability of free space and I_1 is the current in the coil. The equivalent current in the magnet is defined as $I_2 = B_r l_m / (N_m \mu_0)$ representing the relationship between the remanence of the permanent magnet (B_r), the length of the magnet (l_m), and the number of turns in the magnet (N_m), which was selected to be 100 to ensure an even field distribution in the magnet. Furthermore, r_1 represents the radius of the coil, r_2 is the radius of magnet, and x is the axial distance between the center of the coil and the center of the magnet. Finally, $\mathrm{K}(m)$ and $\mathrm{E}(m)$ are the first and second elliptic integrals as a function of m defined as,

$$m = \frac{4 r_1 r_2}{(r_1 + r_2)^2 + x^2}. \quad (2)$$

The total axial force between the coil and permanent magnet can be solved as a function of x by summing the force between individual current-carrying loops across the number of loops in the magnet (N_m), radial layers in the coil (N_r), and axial layers in the coil (N_y) such that,

$$F_{\mathrm{in}}(x) = \sum_{n_m=1}^{N_m} \sum_{n_r=1}^{N_r} \sum_{n_y=1}^{N_y} F_f(r(n_r), R_m, x + L(n_m, n_y)), \quad (3)$$

$$r(n_r) = r_c + \frac{n_r - 1}{N_r - 1}(R_c - r_c), \quad (4)$$

$$L(n_m, n_y) = \frac{n_y - 1}{N_y - 1} l_c + \frac{n_m - 1}{N_m - 1} l_m, \quad (5)$$

where R_m is the radius of the magnet, R_c is the outer radius of the coil, r_c is the inner radius of the coil, l_m is the length of the magnet, and l_c is the length of the coil. From these equations, it is clear that the electromagnetic force output of

TABLE I
COMPARISON OF STATE-OF-THE-ART WEARABLE HAPTIC ACTUATORS.

Actuator Design	Form	Bandwidth	Force
Shape memory alloy [15]	bracelet	>1 Hz*	15 N
Pneumatic elastic tubes [13]	sleeve	3 Hz	1.6 N
Voice coil [29]	sleeve	5 Hz*	2 N
Pneumatic bellows [12]	bracelet	7.1 Hz	10 N
Electric vibration and cable-driven [9]	bracelet	10 Hz	15 N
Electromagnetic solenoid [19]	glove	20 Hz	0.2 N
Hydro-electrostatic [25]	finger tip	<100 Hz	0.3 N
Hydro-electromagnetic (This Work)	bracelet	30 Hz	5.2 N

*Full bandwidth not characterized, maximum operating frequency is quoted.

the coil is nonlinear and that the maximum force is achieved when the coil and magnet are in contact.

To hydraulically amplify force, incompressible fluid assumptions and Pascal's law are used. Here, the incompressible fluid (water) directly transfers forces generated by the electromagnet (F_{in}) at the input area (A_{in}) to the output area (A_{out}). The force applied to the wearer of the device (F_{out}) is then proportional to the ratio of the areas through the pressure,

$$P = \frac{F_{out}}{A_{out}} = \frac{F_{in}}{A_{in}}. \tag{6}$$

Note that the output area is not constant due to the flexibility of the material and may change depending on loading and mounting. Furthermore, because the volume of fluid is constant, a direct trade-off is made between force and stroke at the input and output. Thus, force amplification and actuation stroke can be tuned by altering the area ratio.

Output force can also be increased by increasing the current supplied to the electromagnetic actuator. This, however, can result in higher operating temperatures that can potentially harm the user. Assuming a low Biot number, a lumped capacitance model can be used to estimate the temperature T as a function of time using,

$$T(t) = \frac{I^2 R}{hA_s}\left(1 - e^{\frac{-hA_s}{\rho V c_p}t}\right) + T_0. \tag{7}$$

In this equation, the convection coefficient to the ambient air is h, the surface area of the composite actuator is A_s, the volume is V, the density is ρ, the heat capacity is c_p, and ambient temperature is T_0. Additionally, the heat generated by the coil is $I^2 R$ with a temperature-dependent coil resistance of $R = R_0(1 + \alpha(T - T_0))$, where the temperature-dependent resistivity is α and the room temperature resistance is R_0. By surrounding the electromagnetic actuator with liquid from the hydraulic amplification system, the surface area of the composite actuator increases drastically, leading to improved heat transfer and reduced temperatures. At the same time, a high liquid conductivity k can lead to a low Biot number $Bi \approx hV/(kA_s)$, which improves heat removal from the coil and distributes the heat more evenly across the actuator area. Water, a biocompatible liquid with a high thermal conductivity ($0.60 \, \text{W/m} \cdot \text{K}$) [31], can be used to achieve reduced actuator temperature as well as hydraulic force amplification.

III. ACTUATOR DESIGN AND MANUFACTURING

Using these principles, a simple, scalable hybrid hydro-electromagnetic actuator is designed with an easy-to-manufacture trapezoidal shape, which was chosen to increase the output area with respect to the input area. The overall length of the actuator is 75 mm and the widths are 30 mm and 45 mm at the ends closest to the input and output, respectively.

Figure 2 illustrates the process for fabricating the actuator. To encapsulate water for the hydraulic amplification system, a flexible but inextensible thin-film material is chosen. Not only must this material conform to the human body but it must also transfer forces to the user without attenuation, require low forces to change shape, and minimize risk due to rupture. Additionally, the material needs to be water-tight and non-porous. Several heat-sealable films, shown in Table II, were

TABLE II
PROPERTIES OF POTENTIAL ENCAPSULATION MATERIALS

	COPP	Stretchlon®	Nylon TPU
Evaporation (g/s)	4.6×10^{-8}	3.18×10^{-6}	2.66×10^{-6}
Tensile strength (MPa)	294	55	42*
Elongation at break (%)	50	500	670*
Melting Temperature (°C)	160	120-170	160-200

*Based on properties in [32].

considered for the development of this actuator including co-extruded oriented polypropylene (COPP), stretchlon, and ripstop nylon with thin thermoplastic polyurethane (TPU). The low water-permeability and high tensile strength made COPP the most favorable choice. Additionally, when used at below 30% of the ultimate tensile strength (75 MPa), the fatigue failure of oriented polypropylene plastics is well-beyond 10^6 cycles [33]. Thus, the COPP material is not expected to fail under the maximum designed loading condition of 15 MPa in tension at the magnet and COPP interface.

To create the actuation system, an off-the-shelf electromagnetic coil ($R = 0.32 \, \Omega, L = 27.1 \, \mu\text{H}$) with an inner radius ($r_c$) of 2.25 mm, an outer radius (R_c) of 7 mm, and a length (l_c) of 1.7 mm is used. The coil is mechanically bonded to a COPP bobbin by applying heat and pressure. As the plastic melts, it conforms to the shape of the electromagnet filling in the core and gaps between wires, thereby improving heat transfer. Next, a sheet of 0.02 mm thick COPP is cut on a Epilog Helix laser engraver to the shape shown in Figure 2(B). The electromagnet is then bonded to it by melting the plastic together. Two NdFeB magnets with a radius (R_m) of 6.35 mm and thickness (l_m) of 3.175 mm are then attached to the COPP sheet via mutual magnetic attraction. The location of the bonding points for the electromagnetic components are chosen to maximize the output area A_{out} and maintain close proximity between the coil and magnets.

Next, the COPP sheet is symmetrically folded to align the magnet and electromagnet. The sides are then closed with an impulse sealer. A silicone tube (ID = 0.5 mm, OD = 1 mm)
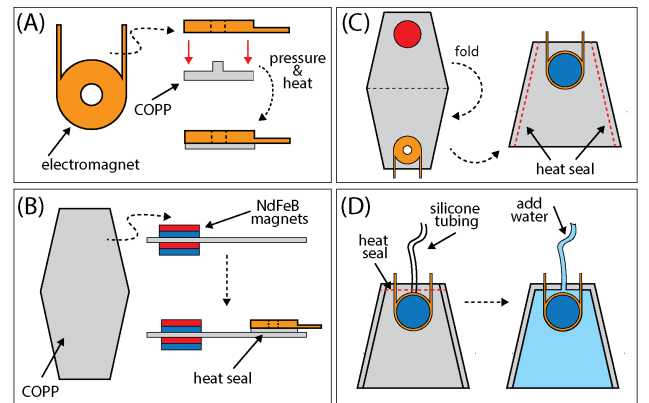
Fig. 2. Manufacturing starts with (A) the electromagnet, which is mechanically bonded to a COPP layer by applying heat and pressure. (B) Next, a pre-cut sheet of COPP is placed between two magnets. The electromagnet is then attached by applying heat to bond the COPP together. (C) The actuator is folded to align the permanent magnets with the electromagnet and heat sealed along the edges. (D) Silicone tubing is inserted and heat sealed. Finally, water is added to the pouch and the tubing is sealed to prevent leakage.
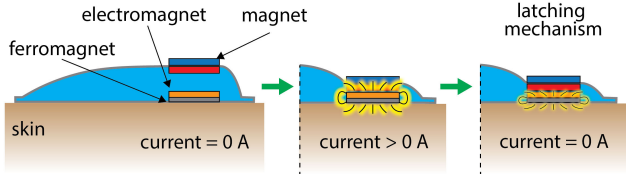
Fig. 3. A latching mechanism using ferromagnetic material is illustrated. When power is supplied to the electromagnet, the permanent magnet attracts to the coil. When power is removed, the force of attraction between the permanent magnet and ferromagnetic material remains, keeping the actuator in the latched state. To detach, the current to the electromagnet is reversed.
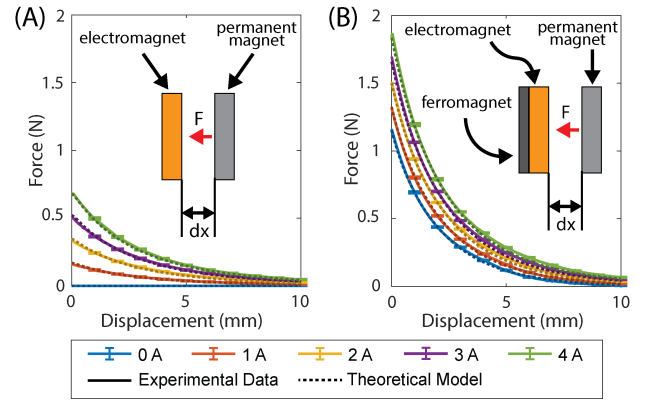

Fig. 4. (A) The force of attraction between the coil and permanent magnet is modeled and measured experimentally for varying levels of input current. (B) The force of attraction is also measured and modeled for the latching design.

is inserted into the open end of the pouch and heat sealed, ensuring that the pouch remains water-tight. Finally, a syringe is inserted into the silicone tube and water is injected into the pouch. The total actuator mass is 5.0 g and the maximum fill volume is 16.5 mL. A fill volume of 12 mL was selected for the majority of the characterization measurements due to its ability to provide a high output force. To enable the addition or removal of water, a luer lock valve can be added. Alternatively, the silicone tubing can be sealed and cut after filling.

For sustained force applications, latching designs can be created by integrating thin ferromagnetic components into the electromagnetic actuator [18], [19], [34]. Latching designs can be advantageous for haptics because they only use power during state changes. Figure 3 demonstrates a latching-based HAPSEA concept that uses materials with high magnetic permeability placed underneath the electromagnetic coil. In this design, the permanent magnet is attracted toward the electromagnet and ferromagnetic component (MuMETAL® disc, 14.3 mm diameter, 0.25 mm thickness, 350,000 max permeability) when current is supplied. However, when current is removed, the force of attraction between the permanent magnet and ferromagnetic material holds the magnet in place, creating a fixed haptic output force with no input power. Reversing the direction of current repels the magnet, restoring it to the original state. In a body-grounded haptic actuator, the internal pressure of the actuator increases when it is attached firmly to the wrist or arm. Thus, more force is required to attract the magnet to the coil. Therefore, the bias force generated by a latching ferromagnetic actuator can serve to minimize the power necessary to operate the actuator. By tuning the dimensions and material selection for the ferromagnetic component, it is possible to maximize force output and minimize current.

IV. ACTUATOR CHARACTERIZATION

In order to compare the predicted and measured performance of the actuator prototype, several experiments were conducted to determine the electromagnetic coil output force, the hydraulically-amplified actuator output force, actuator efficiency, actuator bandwidth, and thermal response.

A. Electromagnetic Force Output

To test the output force of the electromagnetic actuator, a 6-axis force/torque sensor (ATI Nano17) and a linear actuator (SMAC LCS25-050-15V1.0R) were attached to the coil and permanent magnet. Figure 4(A) illustrates the force of

attraction between the coil and magnet as a function of the gap distance. As applied current increases, the force output increases linearly. As the gap distance increases, the force decreases in a nonlinear manner. With 4 A of input current, the electromagnet is able to produce approximately 0.7 N of force. These trends are validated against the force model in Eqn. (3), showing a close match. Here, the mean error between the model and the experimental data is 7.3 ± 6.8 mN.

For the latching design in Fig. 4(B), the ferromagnetic material biases the permanent magnet and increases the force output as the gap distance decreases. Because magnetic forces in free-space obey linear superposition, the force with the ferromagnet at 0 A of current can be added directly to the theory and measurement curves in Fig. 4(A) to achieve the curve in Fig. 4(B). In this instance, at an input current of 4 A, a maximum output force of 1.85 N is achieved. The ferromagnetic material contributes 1.15 N of additional attraction force with a gap distance of zero. Thus, to detach the latched permanent magnet, an impulse of 6.6 A is theoretically required for this configuration.

B. Amplified Actuator Force

The force output, and thus the hydraulic amplification of the hydro-electromagnetic actuator is characterized in Fig. 5. Because it is typically challenging to characterize a device with a human in the loop, blocked force characterization [35] was adopted to reliably determine the actuator performance between two flat surfaces. For each test, a latching or non-latching prototype actuator is filled with 12 mL of water and mounted directly to the force sensor. The electromagnet is supplied a continuous current as a linear actuator compresses the soft pouch at a rate of 1 mm/s. When the permanent magnet separates from the electromagnet moving from the closed to the open state, the output force is recorded as the open or unlatch force. This value represents the minimum amount of external force needed to separate the magnet and coil at a given coil current. Then, the linear actuator reverses direction to reduce pressure to the pouch. When the magnet and coil attract moving from the open to the closed state, the output force is recorded. This attraction force represents the maximum amount of external force that can be applied before
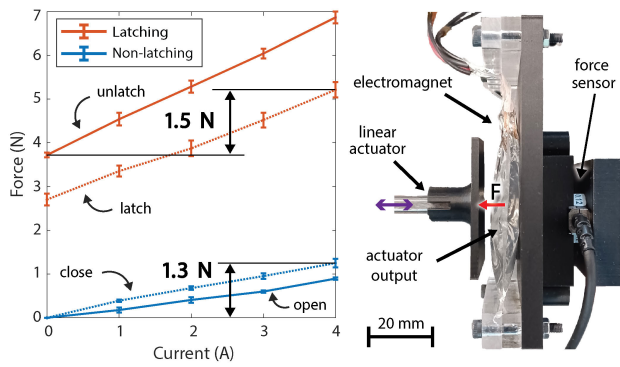
Fig. 5. The threshold forces applied to the pouch that are required to open or close the latching and non-latching actuators are shown. For the 'unlatch' and 'open' curves, the actuator starts in closed state and force required to open the actuator is recorded. For the 'latch' and 'close' curves, the force required to resist the closing motion is shown. A linear actuator is used to adjust the input force and a 6-axis force/torque sensor is used to measure force as current is supplied to the coil.

the actuator is able to close or latch. Hysteresis caused by shape changes in the pouch contact area can be noted in the data, but overall, measurements show high repeatability.

The results shown in Fig. 5 show that the current and force exhibit a linear relationship, which agrees with the analytical model in Section II. At 4 A, the non-latching actuator is able to exert an output force at the pouch that is equal to 1.3 N, which corresponds to a force amplification of $1.9\times$ when compared to the force output of the electromagnet without the fluid pouch. The forces required to close the actuator at different current levels tends to be larger than the force required to open the actuator because the magnet and coil are further apart (2 mm separation) at the start of a close operation.

For the latching actuator at 4 A, the maximum output force at the pouch during a latching operation is approximately 5.2 N with a bias force of 3.7 N to separate from the ferromagnetic plate. The maximum force required to unlatch an actuator at 4 A is 7 N. For this actuator design, the unlatching force is greater than the latching force due to the presence of the ferromagnetic plate. Once preloaded, the actuator can exert an additional 1.5 N force, which corresponds to a force amplification of $2.1\times$ at the pouch. For body-grounded applications, the latching actuator design can be tuned such that the preload force needed to strap the actuator to the body matches the bias force produced by the ferromagnetic plate. Thus, the force bias features of the latching actuator make it more useful than the non-latching actuator for haptic applications.

C. Actuator Efficiency

For low-speed force output applications, the energetic efficiency can be calculated using a full cycle electromechanical modeling technique commonly used for haptic actuators [24], [36]. Here, the actuator is cycled both electrically and mechanically by increasing and decreasing both voltage and external load. Figure 6(A) illustrates this technique. In state 1, the electromagnet is off and a constant load is applied to the output of the system. In the transition between state 1 and state 2, a voltage is applied to the electromagnet and is increased linearly. As the gap between the magnet and electromagnet
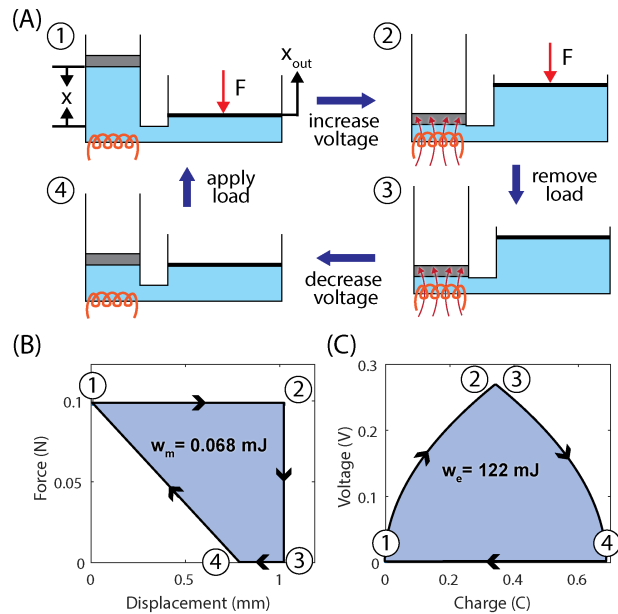

Fig. 6. (A) Full cycle electromechanical efficiency is modeled using a nonlinear electromagnetic force input and Pascal's law to amplify force output. The four states of the cycle are shown as voltage and load are increased and decreased. Efficiency of the hydro-electromagnetic model is estimated by dividing (B) the mechanical work output by (C) the electrical work input. For the current design, an efficiency of 0.056% is estimated.

decreases, the output displacement (x_{out}) increases at a rate proportional to the area ratio. Next, the load is removed, transitioning the system from state 2 to state 3. Then the voltage applied to the electromagnet decreases to zero, bringing the system to state 4, which equalizes the fluid due to hydrostatic pressure. Finally, the load is added again to bring the system back to state 1 in the cycle.

This model uses the measured electrical characteristics, hydraulic amplification, and range-of-motion of the actuator and assumes a constant area ratio, low damping, and no elastic effects to estimate the full cycle electromechanical efficiency. As the actuator is cycled, the output force and displacement are recorded as shown in Figure 6(B). The mechanical work output achieved by the actuator is equal to the enclosed area in the force-displacement plane, which is the integral of force over a known displacement. The electrical energy is determined by the voltage and current (charge is the integral of current) applied to the electromagnet over time, which is equal to the enclosed area in the voltage-charge plane in Figure 6(C).

The total electromechanical efficiency is the ratio of mechanical work output to electrical power consumed and depends highly on loading and initial conditions. For example, to displace a 0.1 N load a distance of 1 mm, the estimated efficiency from the full-cycle electromechanical method is 0.056%. This efficiency range places HAPSEA above phase changing soft actuators (0.0008% to 0.0018%), but well below polymer fiber (1.32%) and HASEL (19.4%) actuators [24], [36], [37]. Generally, electromagnetic actuators are known to have high energetic efficiencies. However, efficiencies can be severely reduced when energy cannot be stored in kinetic or potential forms or in cases with low speeds and long strokes [38], eccentric rotary loads [39], or vibrational op-

erating conditions [40]. Improving the efficiency of HAPSEA may be possible by increasing the strength of the permanent magnet, increasing the area ratio, or reducing the stroke length of the actuator.

D. Dynamic Response

To characterize the dynamics of the soft actuator in air and determine the actuation bandwidth, a laser displacement sensor (Acuity AR100-50mm) is used to measure the movement at the center of the pouch in an unloaded, non-latching actuator with varying levels of fill volume. Because of the nonlinear nature of the force to displacement relationship in this actuator, stochastic system identification methods produced noisy and difficult to interpret results. Thus, the frequency response of the actuator was characterized by testing each frequency separately. A 1 A current square wave is supplied at varying frequencies and at each test condition, a fast Fourier transform is used to isolate the amplitude of the input current at the switching frequency and output displacement at that same frequency. Figure 7 shows the resulting amplitude response.

From these measurements, it is clear that the dynamics of the pouch are dependent on fill volume. This indicates that the incompressible fluid and film increase the stiffness of the actuator at higher volumes. Between 10 and 25 Hz, a resonance is noted in all curves, which is likely caused by fluid oscillations inside the pouch. Contact with human skin, damping, and preloading are likely to alter the dynamic response during use. Overall, however, this soft actuator has a high bandwidth of $\leq$30 Hz for volumes of 8 mL and greater and is able to produce 10 μm vibrations at up to 200 Hz with 1 A of input current.

E. Thermal Response

In addition to hydraulic amplification, the liquid serves as a thermal reservoir that increases the heat transfer area and reduces the risk of thermal failure. Figure 8(A) illustrates the difference between the maximum actuator temperature with and without water cooling. Here, the electromagnet is powered in ambient air at 26 °C and the liquid pouch contains 10 mL of water. Both actuators are powered continuously with 2 A

for 120 seconds and the temperature gradient of the COPP material (emissivity of 0.94 for the bobbin and pouch [41]) is recorded with a FLIR thermal camera (128 $\times$ 96 pixels). The maximum temperature of the system is recorded and plotted as a function of time. In air, the electromagnet reaches a temperature of 112 °C at 120 s with the temperature increasing at a rate of 0.35 ± 0.08 °C/s. Conversely, the electromagnet in water reached a steady peak temperature of 36 °C at 120 s with negligible temperature increase. This steady state temperature increase is small (10 °C) and close to human body temperature, illustrating that it can be safe to operate for long-term haptics. Additionally, to increase comfort for users, the actuator can be preheated from room temperature to skin temperature in less than 30 seconds. Figure 8(C) shows the contrast in temperatures at 120 s and highlights the advantages of using the hydraulic system for reducing temperatures.

One of the reasons for the continuous rise in temperature in the air cooling system is the temperature-dependent resistivity of copper ($\alpha = 0.4$ %/°C). Figure 8(B) illustrates this effect. As the temperature of the coil increases, the resistance also increases further accelerating the temperature rise. In fact, this mechanism makes the apparent time constant of the air cooling system estimated in Eqn. (7) appear significantly longer than the water cooling system. By integrating the temperature-dependent resistance into Eqn. (7), the theoretical model shown in Fig. 8(A) is produced. Here, the geometric properties of the coil and pouch are used to determine the volume and surface area of the respective systems. The convection coefficient is estimated to be 40 to 50 W/m^{2}K and the density and specific heat for water and copper are used.

Overall, results show that the resistance of the coil in air increases by 36% over 120 s, whereas the system with water only changed by 4%. Since heat generation increases linearly with power and resistance ($P = I^2R(T)$) and efficiency is a function of power, a higher operating temperature leads to a less efficient actuator. Therefore, maintaining low temperatures also improves actuator efficiency.

Fig. 8. (A) The maximum temperature and (B) resistance of an electromagnet are measured in open air and in water with 2 A of continuously applied current. (C) Thermal images are illustrated for the two systems at 120 s. The coil in water maintained a much lower temperature, making it more suitable for haptic applications.
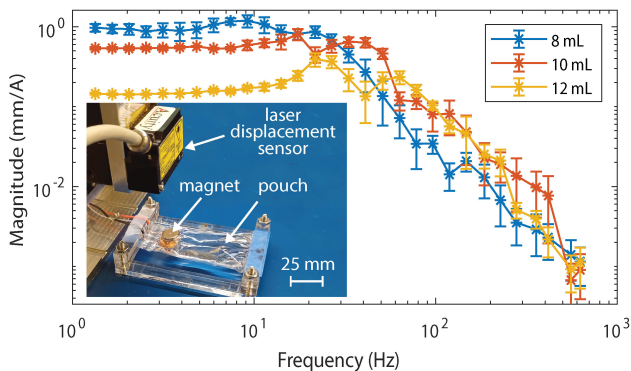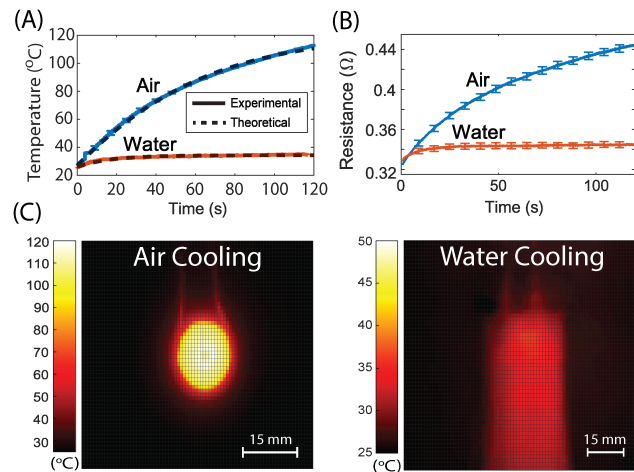

Fig. 7. Frequency responses of the pouch operating in air with varying fill volumes are captured using a laser displacement sensor. The transfer function (mm/A) is estimated at varying frequencies.

V. HAPTIC DEVICE APPLICATION

To demonstrate how the hydraulically amplified system can be used for a haptic wrist device, five latching HAPSEAs are assembled together. Figure 9 shows the design and function of the device. Here, the actuators are assembled in alternating orientation to reduce magnetic interference and to maintain the rectangular profile. At the ends of the device, hook and loop fabric as well as a thin elastic portion are attached, making it comfortable, adjustable, and easy to don and doff. By wrapping the assembly around the wrist, each actuator is mechanically grounded to the body and preloaded. To reduce risk of electrical shorts, the electromagnets are soldered directly to the power connections. Furthermore, the voltages supplied through each actuator are very low (<5 V) and the electrical resistance of human skin is very high (>1000 Ω). Thus, this actuation scheme is relatively safe to operate around human users [42].

To control the haptic device, each of the five actuators are connected to a motor controller (Pololu G2 18V17) that is individually controlled by a microcontroller (Arduino Uno Rev3). Various modalities of haptic feedback can be achieved through this prototype device. Figure 9(B-D) demonstrates a squeeze mode where all the actuators are simultaneously energized to apply force directly to the wrist, a local force mode where individual actuators are addressed, and a vibration mode where the actuators are oscillated at a frequency up to 200 Hz. Other unique modes can also be achieved by energizing actuators in series to create a ripple effect. Results in supplemental Video 1 illustrate how the actuator can be used as a wrist haptic device. With the ability to generate multiple haptic modes, future iterations of HAPSEA actuators could be used in AR/VR applications to interact with objects and environments, receive alerts and notifications, or give the sensation of touch to improve immersion.

VI. CONCLUSION

In this work, we demonstrate a novel electromagnetic actuator that is hydraulically amplified in order to increase output force and decrease operating temperatures. The actuator has a low-cost and an easy-to-manufacture architecture, using a simple geometry, heat sealable materials, and water as the hydraulic fluid. In order to provide extra biasing forces when worn and enable higher efficiencies during operation, a latching version is also implemented. To better understand the design space, simple electromagnetic force, hydraulic amplification, and temperature models are developed. These models are then compared with experimental data and a prototype haptic wrist device is demonstrated.

Overall, the soft actuator shows high force, high bandwidth, and low temperature operation. Forces of 5.2 N are generated at the output of the actuator at 4 A with a preload of 3.7 N. In general, the actuator is able to exert a net force of 1.5 N, which is a $2\times$ amplification of the electromagnetic input force. In open air, this prototype actuator achieved a bandwidth of ≥ 30 Hz and stroke length of 0.4 mm operating at 1 A and 12 mL of fill volume. Additionally, the actuator is able to generate amplitudes greater than 10 μm at 200 Hz, which shows potential for use in wearable devices. With electromagnetic actuators, extended use often causes overheating or failure. With the addition of the hydraulic amplification system, the heat transfer surface area is greatly increased leading to a significant decrease in temperature. With continuous 2 A operation, the steady state temperature was 36 °C.

There are several future alterations that could further improve the actuator for haptic applications. More complex designs that restrict the motion of the magnet, reduce the gap between the coil and magnet, and a ferromagnetic yoke to direct magnetic field lines can greatly improve the force output of the electromagnet. More complex pouch designs and heat-sealable geometries can also improve range-of-motion, amplification, linearity, and hysteresis.

Finally, as in many other electromechanical systems, higher efficiencies are achieved as a result of the dynamic transfer of energy between potential and kinetic elements. Thus, the efficiency of this soft actuator (and battery life of the haptic device) can also be further improved by operating at resonant frequencies.

Overall, this work demonstrates a novel concept for developing next-generation haptic actuators that are low-cost, easy to manufacture, high force, high bandwidth, and low operating temperature. When incorporated into haptic devices, the actuators can generate a variety of sensations including squeeze, local forces, and vibrations. With further development and miniaturization, future iterations of HAPSEA actuators could eventually be implemented for everyday human-robot interfaces, wearables, and AR/VR applications.
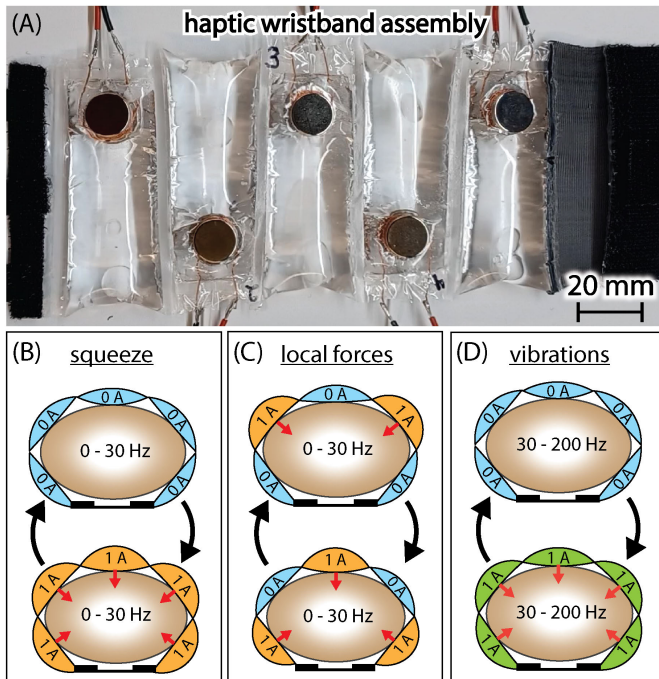

Fig. 9. (A) The design for a wearable haptic device is illustrated with five soft actuators. Several modalities can be achieved with the device including (B) uniform squeeze by actuating all HAPSEAs at low frequencies, (C) local forces by actuating individual HAPSEAs, and (D) vibrations by actuating HAPSEAs at high frequencies.

REFERENCES

[1] P. Richard, G. Birebent, P. Coiffet, G. Burdea, D. Gomez, and N. Langrana, "Effect of frame rate and force feedback on virtual object manipulation," *Presence: Teleoperators & Virtual Environments*, vol. 5, no. 1, pp. 95–108, 1996.

[2] K. J. Kuchenbecker, J. Fiene, and G. Niemeyer, "Improving contact realism through event-based haptic feedback," *IEEE Transactions on Visualization and Computer Graphics*, vol. 12, no. 2, pp. 219–230, 2006.

[3] V. Hayward, O. R. Astley, M. Cruz-Hernandez, D. Grant, and G. Robles-De-La-Torre, "Haptic interfaces and devices," *Sensor Review*, 2004.

[4] Y. Visell, "Tactile sensory substitution: Models for enaction in HCI," *Interacting with Computers*, vol. 21, no. 1-2, pp. 38–53, 2009.

[5] E. Pezent, A. Gupta, H. Duhaime, M. O'Malley, A. Israr, M. Samad, S. Robinson, P. Agarwal, H. Benko, and N. Colonnese, "Explorations of wrist haptic feedback for AR/VR interactions with Tasbi," in *Adjunct Proceedings of the 35th Annual ACM Symposium on User Interface Software and Technology*, 2022.

[6] M. A. Baumann, K. E. MacLean, T. W. Hazelton, and A. McKay, "Emulating human attention-getting practices with wearable haptics," in *2010 IEEE Haptics Symposium*, 2010, pp. 149–156.

[7] A. A. Stanley and K. J. Kuchenbecker, "Design of body-grounded tactile actuators for playback of human physical contact," in *2011 IEEE World Haptics Conference*, 2011, pp. 563–568.

[8] ——, "Evaluation of tactile feedback methods for wrist rotation guidance," *IEEE Transactions on Haptics*, vol. 5, no. 3, pp. 240–251, 2012.

[9] E. Pezent, A. Israr, M. Samad, S. Robinson, P. Agarwal, H. Benko, and N. Colonnese, "Tasbi: Multisensory squeeze and vibrotactile wrist haptics for augmented and virtual reality," in *2019 IEEE World Haptics Conference (WHC)*, 2019, pp. 1–6.

[10] K. Chubb, D. Berry, and T. Burke, "Towards an ontology for soft robots: what is soft?" *Bioinspiration & Biomimetics*, vol. 14, no. 6, p. 063001, 2019.

[11] J. Yin, R. Hinchet, H. Shea, and C. Majidi, "Wearable soft technologies for haptic sensing and feedback," *Advanced Functional Materials*, vol. 31, no. 39, p. 2007428, 2021.

[12] E. M. Young, A. H. Memar, P. Agarwal, and N. Colonnese, "Bellowband: A pneumatic wristband for delivering local pressure and vibration," in *2019 IEEE World Haptics Conference (WHC)*, 2019, pp. 55–60.

[13] M. Zhu, A. H. Memar, A. Gupta, M. Samad, P. Agarwal, Y. Visell, S. J. Keller, and N. Colonnese, "Pneusleeve: In-fabric multimodal actuation and sensing in a soft, compact, and expressive haptic sleeve," in *Proceedings of the 2020 CHI Conference on Human Factors in Computing Systems*, 2020, p. 1–12.

[14] H. Jin, Y. Ouyang, H. Chen, J. Kong, W. Li, and S. Zhang, "Modeling and motion control of a soft SMA planar actuator," *IEEE/ASME Transactions on Mechatronics*, vol. 27, no. 2, pp. 916–927, 2022.

[15] A. Gupta, A. A. R. Irudayaraj, and R. Balakrishnan, "HapticClench: Investigating squeeze sensations using memory alloys," in *Proceedings of the 30th Annual ACM Symposium on User Interface Software and Technology*, 2017, p. 109–117.

[16] Q. Ding, J. Chen, W. Yan, K. Yan, A. Kyme, and S. S. Cheng, "A high-performance modular SMA actuator with fast heating and active cooling for medical robotics," *IEEE/ASME Transactions on Mechatronics*, vol. 27, no. 6, pp. 5902–5913, 2022.

[17] J. Jeong, K. Hyeon, J. Han, C. H. Park, S.-Y. Ahn, S.-K. Bok, and K.-U. Kyung, "Wrist assisting soft wearable robot with stretchable coolant vessel integrated SMA muscle," *IEEE/ASME Transactions on Mechatronics*, vol. 27, no. 2, pp. 1046–1058, 2022.

[18] V. Vechev, J. Zarate, D. Lindlbauer, R. Hinchet, H. Shea, and O. Hilliges, "Tactiles: Dual-mode low-power electromagnetic actuators for rendering continuous contact and spatial haptic patterns in VR," in *2019 IEEE Conference on Virtual Reality and 3D User Interfaces (VR)*, 2019, pp. 312–320.

[19] F. Pece, J. J. Zarate, V. Vechev, N. Besse, O. Gudozhnik, H. Shea, and O. Hilliges, "MagTics: Flexible and thin form factor magnetic actuators for dynamic and wearable haptic feedback," in *Proceedings of the 30th Annual ACM Symposium on User Interface Software and Technology*, 2017, p. 143–154.

[20] S. R. Doerger and C. K. Harnett, "Force-amplified soft electromagnetic actuators," *Actuators*, vol. 7, no. 4, 2018.

[21] N. Kohls, B. Dias, Y. Mensah, B. P. Ruddy, and Y. C. Mazumdar, "Compliant electromagnetic actuator architecture for soft robotics," in *2020 IEEE International Conference on Robotics and Automation (ICRA)*, 2020, pp. 9042–9049.

[22] N. Kohls, I. Abdeally, B. P. Ruddy, and Y. C. Mazumdar, "Design of a Xenia coral robot using a high-stroke compliant linear electromagnetic actuator," *ASME Letters in Dynamic Systems and Control*, vol. 1, no. 3, 2021, 031011.

[23] N. D. Kohls, R. Balak, B. P. Ruddy, and Y. C. Mazumdar, "Soft electromagnetic motor and soft magnetic sensors for synchronous rotary motion," *Soft Robotics* [In Press], 2023.

[24] S. K. Mitchell, X. Wang, E. Acome, T. Martin, N. Ly, N. Kellaris, V. G. Venkata, and C. Keplinger, "An easy-to-implement toolkit to create versatile and high-performance HASEL actuators for untethered soft robots," *Advanced Science*, vol. 6, no. 14, p. 1900178, 2019.

[25] E. Leroy, R. Hinchet, and H. Shea, "Multimode hydraulically amplified electrostatic actuators for wearable haptics," *Advanced Materials*, vol. 32, no. 36, p. 2002564, 2020.

[26] H. Phung, P. T. Hoang, H. Jung, T. D. Nguyen, C. T. Nguyen, and H. R. Choi, "Haptic display responsive to touch driven by soft actuator and soft sensor," *IEEE/ASME Transactions on Mechatronics*, vol. 26, no. 5, pp. 2495–2505, 2021.

[27] F. Chen, K. Liu, Q. Pan, S. Chen, and X. Zhu, "An integrated design and fabrication strategy for planar soft dielectric elastomer actuators," *IEEE/ASME Transactions on Mechatronics*, vol. 26, no. 5, pp. 2629–2640, 2021.

[28] J. W. Park, J.-H. Yang, and H. Kim, "A large-deflection high-force micro electromagnetic hydraulic latex membrane actuator for fluid manipulation in micro channels," in *2011 IEEE 24th International Conference on Micro Electro Mechanical Systems*, 2011, pp. 1209–1212.

[29] H. Culbertson, C. M. Nunez, A. Israr, F. Lau, F. Abnousi, and A. M. Okamura, "A social haptic device to create continuous lateral motion using sequential normal indentation," in *2018 IEEE Haptics Symposium*, 2018, pp. 32–39.

[30] W. Robertson, B. Cazzolato, and A. Zander, "Axial force between a thick coil and a cylindrical permanent magnet: Optimizing the geometry of an electromagnetic actuator," *IEEE Transactions on Magnetics*, vol. 48, no. 9, pp. 2479–2487, 2012.

[31] D. Ibrahim and C. Zamfirescu, *Drying phenomena: Theory and applications*. John Wiley & Sons, Ltd, 2016.

[32] S. Jiang, G. Duan, H. Hou, A. Greiner, and S. Agarwal, "Novel layer-by-layer procedure for making nylon-6 nanofiber reinforced high strength, tough, and transparent thermoplastic polyurethane composites," *ACS Applied Materials & Interfaces*, vol. 4, no. 8, pp. 4366–4372, 2012.

[33] N.-M. Barkoula, B. Alcock, N. Cabrera, and T. Peijs, "Fatigue properties of highly oriented polypropylene tapes and all-polypropylene composites," *Polymers and Polymer Composites*, vol. 16, 2008.

[34] R. Balak and Y. C. Mazumdar, "Bistable valves for magnetorheological fluid-based soft robotic actuation systems," *Robotics and Automation Letters*, vol. 6, no. 4, pp. 8285–8292, 2021.

[35] S. Taccola, F. Greco, E. Sinibaldi, A. Mondini, B. Mazzolai, and V. Mattoli, "Toward a new generation of electrically controllable hygromorphic soft actuators," *Advanced Materials*, vol. 27, no. 10, pp. 1668–1675, 2015.

[36] J. Li, M. Sun, and Z. Wu, "Design and fabrication of a low-cost silicone and water-based soft actuator with a high load-to-weight ratio," *Soft Robotics*, vol. 8, no. 4, pp. 448–461, 2021.

[37] C. S. Haines, M. D. Lima, N. Li, G. M. Spinks, J. Foroughi, J. D. W. Madden, S. H. Kim, S. Fang, M. J. de Andrade, F. Göktepe, Özer Göktepe, S. M. Mirvakili, S. Naficy, X. Lepró, J. Oh, M. E. Kozlov, S. J. Kim, X. Xu, B. J. Swedlove, G. G. Wallace, and R. H. Baughman, "Artificial muscles from fishing line and sewing thread," *Science*, vol. 343, no. 6173, pp. 868–872, 2014.

[38] J. McBean and C. Breazeal, "Voice coil actuators for human-robot interaction," in *2004 IEEE/RSJ International Conference on Intelligent Robots and Systems (IROS)*, vol. 1, 2004, pp. 852–858.

[39] M. Rigacci, R. Sato, and K. Shirase, "Evaluating the influence of mechanical system vibration characteristics on servo motor efficiency," *Precision Engineering*, vol. 72, pp. 680–689, 2021.

[40] H. Yaguchi and Y. Itoh, "Vibration actuator system with small-scale size capable of visual inspection of large complex iron structures," *Applied Sciences*, vol. 11, no. 16, 2021.

[41] A.-L. Davesne, T. Bensabath, J. Sarazin, S. Bellayer, F. Parent, F. Samyn, M. Jimenez, F. Sanchette, and S. Bourbigot, "Low-emissivity metal/dielectric coatings as radiative barriers for the fire protection of raw and formulated polymers," *ACS Applied Polymer Materials*, vol. 2, no. 7, pp. 2880–2889, 2020.

[42] R. M. Fish and L. A. Geddes, "Conduction of electrical current to and through the human body: a review," *Eplasty*, vol. 9, p. e44, 2009.

Noah Kohls received his B.S. in Mechanical Engineering in 2019 from the University of Cincinnati, Cincinnati, OH, USA and his M.S. in Mechanical Engineering in 2022 from Georgia Institute of Technology, Atlanta, GA, USA. He is currently a Ph.D. candidate in Robotics at Georgia Tech.

His research interests include the design and control of soft robotic systems that use soft electromagnetic actuators and sensor topologies. He is also interested in the development of novel soft systems for haptic feedback.

Nicholas Colonnese received his B.S. in Mechanical Engineering in 2009 from the University of Washington and his M.S. (2012) and Ph.D. (2015) in Mechanical Engineering from Stanford University.

He is currently a Research Science Director at Meta Reality Labs Research, working on novel interfaces for augmented and virtual reality. He leads a multidisciplinary haptic displays program, which includes researchers with expertise in materials, actuation, rendering algorithms, perception, interaction design, and haptic value evaluation.

"Ellen" Yi C. Mazumdar (M'09–SM'21) received her B.S., M.S., and Ph.D. degrees in Mechanical Engineering from Massachusetts Institute of Technology, Cambridge, MA, USA in 2008, 2010, and 2015, respectively. She was a Postdoctoral Appointee at Sandia National Laboratories in Albuquerque, NM. Since 2019, she has been an Assistant Professor in the School of Mechanical Engineering with a courtesy appointment in the School of Aerospace Engineering at Georgia Institute of Technology, Atlanta, GA. Her research interests include the development of soft robots, magnetic measurement techniques, optical diagnostics, and new sensor materials for the study of complex physical phenomena.
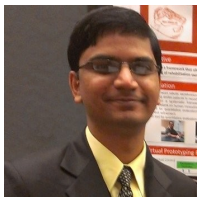
Priyanshu Agarwal received his B.Tech from the Motilal Nehru National Institute of Technology, India in 2007, M.S. degree from the State University of New York, Buffalo, NY, USA in 2012 and Ph.D. degree from the University of Texas at Austin, Austin, TX, USA, in 2017, all in Mechanical Engineering.

He is currently a Research Scientist at Meta Reality Labs Research, where he is leading research on novel haptic interfaces for virtual and augmented reality applications.